Bubble dislodgment in a capillary network with microscopic multi-channel and multi-bifurcation features

Bubble dislodgment in a capillary network with microscopic multi-channel and multi-bifurcation features

Cong Chao[1], Xiaoqiang Jin[1], Lijun Teng[2], Adam A Stokes[2], Xianfeng Fan[1*]

1. Institute for Materials and Processes, School of Engineering, The University of Edinburgh, The King's Buildings, Robert Stevenson Road, Edinburgh, EH9 3FB, UK
2. Institute for Integrated Micro and Nano Systems, School of Engineering, The University of Edinburgh, The King's Buildings, Alexander Crum Brown Road, Edinburgh, EH9 3FB, UK

[*]Corresponding Author Email: x.fan@ed.ac.uk

Abstract

Bubble lodgment in complex capillary network is a common issue in many industrial and biological processes. Research work reported in literature only investigated bubble dislodgement in single channels, and did not consider the effect of network complexity on the dislodgement. This paper focuses on the pressure required to dislodge single bubble from a microscopic capillary network, and investigates what factors affecting the dislodging pressure, to facilitate the precise control of bubble flows in porous media. A capillary network with multi-bifurcation and smoothly-changed diameter is designed to closely mimic the structure of the physiological vascular networks. Over 600 bubble dislodgement experiments have been conducted to understand the effect of

network structure, channel dimensions, and bubble length on the dislodging pressure. The results indicate that network structure is a dominant factor affecting the dislodging pressure, and dislodging pressure increases with the increase in network complexity. The effect of bubble length on the dislodging pressure depends on bubble length. When the bubble length is less than a certain value, which is around 2 mm in this study, the dislodging pressure increases significantly with the decrease of bubble length. Once the bubble length is larger than 2 mm, the dislodging pressure is independent of bubble length.

A model has been proposed to explain the bubble dislodgement in complex capillary networks. The impact of network structure on the bubble dislodging pressure is characterized by a parameter c_j. The model indicates that the dislodging pressure is the function of bubble length, channel dimension and network structure. The analysis of model parameters NB_j and MA_j shows that parameter c_j, rather than the channel size dominates the dislodging pressure for bubbles with length greater than 2 mm, and the increase rate of the dislodging pressure is significantly affected by both channel size and parameter c_j.

Key words: Capillary network, Dislodging pressure, Bifurcations, Multichannel, Bubble movement, Diverging angle

Introduction

Understanding of bubble flows in porous media is of particular interest in enhanced oil recovery[1], intravascular gas embolism treatment[2-3], fuel cells[4-6], and chemical reactors[7-8] etc. For example, the infusion of bubbles into liquid can promote the mass or heat transfer in porous media, whereas bubbles may block the microchannel, thus disturb the performance and reduce the efficiency of the fluid transport and migration in microfluidics. In medical applications, embolotherapy a potential cancer treatment, utilizes bubble lodgment to achieve the occlusion of the arteriole or capillary in targeted sites. The lodged bubbles block microvessels to restrict blood supply to tumors, and thus control the growth of tumor cells[2, 9-11]. Another potential cancer treatment-microbubble-loaded drug delivery has been investigated for decades, while the safety issues still hinder its transform from bench to clinics[12]. The precise control of bubble lodgment at the targeted sites will significantly increase therapeutic efficacy of treatment, and decrease the side effects, such as the drug accumulation and distribution in healthy tissues. A thorough understanding of bubble lodgment and dislodgment in complex capillary network helps to control bubble flow in blood vessels, and to improve the feasibility and efficiency of transport, for example, understanding where the bubble ultimately lodges, whether the bubble can be lodged and dislodged properly, and the persistence time of microbubble lodged around the targeted sites[13].

Bubbles flow as tubular bubbles in small blood vessels, and may be lodged in

capillaries, as observed *in vitro* by Calderon et al.[14] and *in vivo* by Samuel et al[11]. Samuel et al. observed that the perfluorocarbon bubbles with an average length of 76 ± 23 μm often lodged at the capillary bifurcation in the rats. In a bifurcation model patterned on poly (dimethyl siloxane) (PDMS), Calderon et al. found that the air bubble commonly lodged at the daughter channel of the bifurcation. They also investigated the impact of bubble size, parent to daughter channel ratio, and cross-sectional shape and area on the bubble lodgment. The two groups also observed that the driving pressure required to dislodge the bubble is much higher than the lodging pressure. In order to precisely control the bubble flow in a capillary network, it is worth to investigate the pressure required to dislodge the bubble, and what factors affecting the bubble dislodgment in a capillary network.

Some work has been done to investigate the bubble dislodgment in single microchannel. Blackmore et al. studied the bubble adhesion and detachment experimentally between two parallel plates with a width of 11 mm and a thickness of 30-200 μm, and demonstrated that the effect of D_c/h (D_c is bubble contact diameter, and h is the channel height) on the capillary number required to detach a bubble[15]. They found that the shearing force required to dislodge a bubble decreased with the increase of bubble contact length. The liquid they used was engine oil and the channel surface was hydrophobic. As the channel width in their study was 11 mm in diameter, bubble flow condition and bubble dislodgment may be significantly different from that in microscopic capillary

network. Mohammadi and Sharp modelled the pressure difference required to dislodge ‘dry’ bubbles in straight microchannel with a height and width of around 980 μm[16]. However, in their modelling, the drag force and viscous force were neglected and the pinning force was assumed as the only resistant force acting on ‘dry’ bubbles, which may not reflect the real flow conditions and the forces applied on the bubble in capillary networks. In addition, surface tension of the liquid[17] and channel surface properties (roughness, chemical heterogeneities[18]) should affect the bubble dislodgment in microchannel, but were not taken into account in their modelling.

Few study was performed to investigate bubble dislodgment in complex capillary network. The network structures reported in literatures for the investigation into bubble flow behavior are mainly single straight channels[6, 13, 16], Y-type or U type channels[3, 19-21]. A single channel cannot simulate the flow conditions of bubble lodgment in complex capillary network. For example, when an elongated bubble lodges in a single cylindrical channel, the pressure difference between the two ends of the bubble is the driving force to push the bubble, as there is no other pathway for the liquid to move forwards. However, a capillary network has many bifurcations. Fluids in a network have several paths to choose, and will consciously travel to the channel with smaller resistance (without bubbles/with less bubbles). In this case, the bubble will be more difficult to dislodge. Capillary network with multi-bifurcation is able to demonstrate the effect of multichannel and bifurcations on the flow resistance

and bubble dislodgment. Previous studies on bifurcation model mainly investigated the bubble splitting and to which daughter tubes the bubble would travel[3, 19-20, 22]. A tree-like structure, which is the most complicated network reported in literature, has been intensively investigated for mixing efficiency, pressure drop, mass and heat transfer rate in the applications of electronics cooling[23], fuel cells[24] and chemical reactors[25, 26-28]. However, most of the tree-like structures manufactured or simulated in literatures are symmetrical dichotomous, which have straight channels and junctions without smooth change.

In this study, the capillary network is designed with smooth flowpath to closely mimic the structure of the physiological vascular networks[29]. The designed network is featured by multi-channel and multi-bifurcation. The distribution of branching channel size nearly obeys the Murray's law, which is the basic principle for designing transfer networks. This paper investigates the effect of channel complexity, diverging/converging angles, channel dimensions, and bubble length on the bubble flow resistance and bubble dislodging pressure in the capillary network. A theoretical model has been established to illustrate the underlying physics of bubble dislodgement in a capillary network, and to specify the relationship between bubble length and dislodging pressure. The effects of surface tension, viscosity, surface roughness, contact angle and thin film deposition have been considered in the model.

Theory

Bubble dislodgement from a microchannel is governed by the forces acting upon the bubble. The dominant forces involved are buoyancy force, drag force, viscous force, and surface tension acting around the bubble contact line. Drag force is exerted by the pressure difference between two ends of the bubble and the corner flow on the bubble in the rectangular channel[30]. The buoyancy force is constant as the bubble volume is fixed (the gas is taken as incompressible under the experimental condition). The inertial effect of the bubble is neglected due to the low *We* number (less than 1)[16, 20, 31]. Capillary number ($Ca = \frac{\mu u}{\gamma}$) in this work is approximately in an order of 10^{-4}, which is similar to the capillary number in the human circulatory system (smaller than 10^{-3} for microvessels less than 500 μm)[32]. Surface tension around the bubble acts as the 'adhesion force', to 'glue' the bubble onto the surface of the channel[13, 33]. The dislodgment of bubble from a microchannel occurs when pressure difference across the bubble is sufficient to against the resistant pressure drop, which is the sum of the capillary pressure drop and frictional pressure drop.

Capillary pressure drop

The capillary pressure difference across the bubble can be reasonably expressed as the function of surface tension and curvatures of the menisci based on Young–Laplace equation as reported in many literatures[34-37]. At the initial movement of the bubble, the curvature of menisci can be taken as the

function of the cross-sectional area of the microchannel, the advancing and receding contact angle. For a rectangular microchannel, the capillary pressure drop ΔP_c could be expressed by equation (1)[16, 38],

$$\Delta P_c = 2\sigma\left(\frac{1}{W_j}+\frac{1}{H_j}\right)(\cos\theta_{rec}-\cos\theta_{adv}) \quad (1)$$

where σ is the surface tension, *W*, *H* is the channel width and height, respectively, and subscript *j* represents the corresponding microchannel.

Frictional pressure drop

According to the lubrication theory, a liquid film exists between the bubble and the channel wall when an elongated bubble moves in a straight channel filled with liquid. This liquid film is uniform between two bubble ends, and it is of order $Ca^{2/3}$ in thickness[30, 39]. Due to the negligible of gravitational force and shear force of gas phase, the liquid film is commonly assumed to be stagnant. The frictional resistance to bubble motion arises from liquid films [40], and the frictional pressure drop for bubble-liquid flow through a channel with a diameter of *D*, can be calculated through Darcy-Weisbach equation[8, 35, 41],

$$\Delta P_f = 2\rho f_f u^2 \frac{\Delta L}{D} \quad (2)$$

where u is the mean superficial velocity, f_f is the frictional factor. In laminar flow (*Re* number is less than 10 in this study), f_f can be estimated through $f_f = \frac{16}{Re_m}$, where Re_m is the Reynolds number of the mixture, given as,

$$Re_m = \frac{\rho u D}{\mu_m} \quad (3)$$

where μ_m is the mixture viscosity, which can be evaluated through many correlations[42-44].

Materials and Method

Experimental setups

The structure of capillary network is designed (Fig. 1b) based on Murray's law, which states that under ideal conditions, when a parent blood vessel branches into daughter vessels, the cube of the radius of the parent vessel is equal to the sum of the cubes of the radii of daughter blood vessels[29]. The capillary network used in this study was engraved on an Acrylic sheet (2mm, Acrylic Cast, AMARI, contact angle is around 68º[45]) with a fusion laser engraving and cutting system (Epilog laser fusion M2). As the leaser cutting cannot make a circular cross section, the shape of the channel cross sections was rectangular in this study. In practice, for example in electronic device, electrodes and porous rocks, the micro-channels are not necessary to have circular cross section. The blood vessels in human body also have non-circular cross-sections according to the anatomic quantifications. The circular shape of blood vessels can distort and change with dilation and constriction[46]. We have considered the effect of the rectangular shape on fluid transport in the modelling section. In rectangular channels, the liquid either pushes the bubble (plug flow), or bypasses the bubble through the corner channels (corner flow). Within the flowrate range used in this study, the flow in polygonal channels obeys the nonlinear pressure-

velocity relation, as flows in circular channels[30, 32, 47]. The channel height (*H*), width (*W*) and length (*L*) were all measured by the microscope, as shown in Table 1.

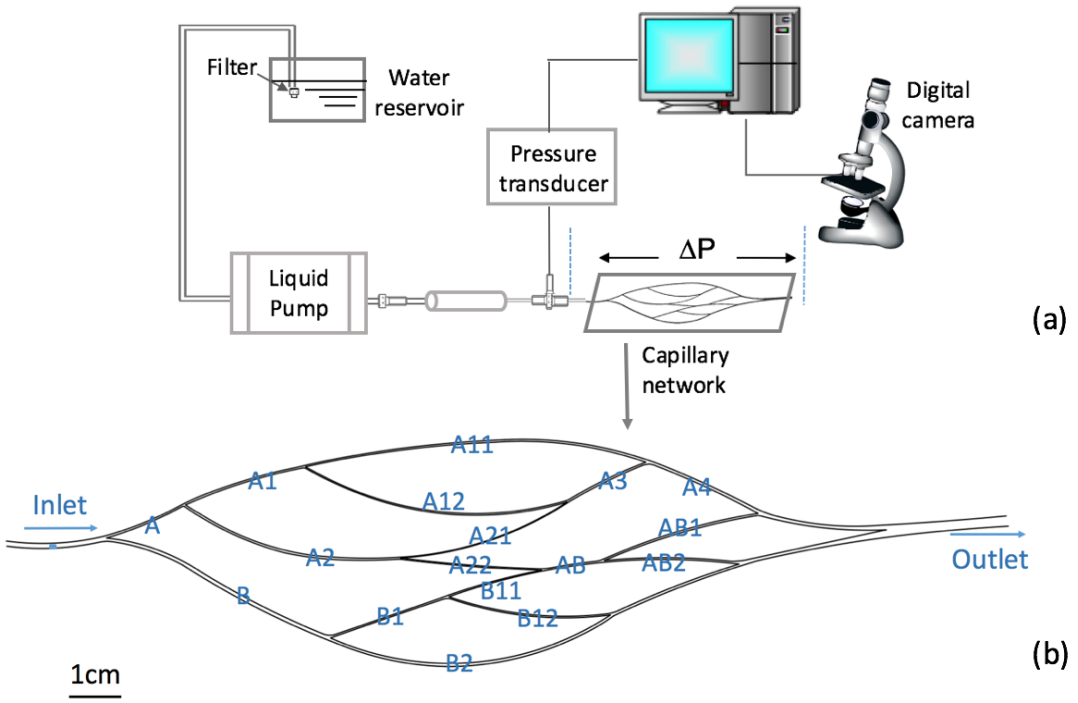

Fig. 1 (a) Schematic of experimental setup, ΔP is the pressure difference between the inlet and outlet of the capillary network; (b) a schematic diagram of the designed capillary network (each channel in capillary network is labelled)

Table 1. Parameters of microchannels in capillary network (The channel height for microchannels listed below is uniform, approximately 0.32 mm)

Channel	Width	Length	Channel	Width	Length

	(mm)	(cm)		(mm)	(cm)
A11	0.46	6.15	AB1	0.45	2.65
A12	0.46	5.05	AB2	0.45	2.4
A2	0.52	4.55	B1	0.40	2.2
A21	0.26	2.95	B11	0.36	1.55
A22	0.37	2.4	B12	0.41	3.0

A liquid delivery pump with a resolution of 0.0001 ml/min (LC-20 AD, Shimadzu) is used to adjust the driving pressure for fluids flow and to control the liquid volumetric flowrate. A digital pressure transducer (DPI 280, Druck) with a resolution of 0.01 mbar is employed to measure the overall pressure drop for fluid flows in the capillary network. The image of bubble motion is recorded through a long working distance microscope (Brunel Microscope Ltd, 10x objective) fitted with a digital camera (AM7023 Dino-Eye, Dino-Lite Digital Microscope).

Measurement of bubble dislodging pressure in the capillary network

In this study, the capillary network was maintained in a horizontal configuration.

A bubble was injected into the capillary network which was initially filled with DI water. The liquid pump was then operated at a flowrate of 0.1 ml/min. At the beginning, the driving pressure across the bubble was low and only for slowly delivering the bubble into the first bifurcation. Once the bubble was stuck in somewhere of a channel, the driving pressure was increased slowly to a point at which the bubble was dislodged from the capillary network. At the moment when the bubble dislodged, the pressure measured over the capillary network was accounted as the dislodging pressure (ΔP). The pressure was recorded at the inlet of the capillary network through the pressure transducer. To eliminate the impact of other bubbles on the measured dislodging pressure, only one bubble was in the network channel for every individual measurement. The pressure drop caused by liquid flows (DI water only) in the capillary network was also measured, as the reference data. Images of bubble was taken through the video-fitted microscope to measure the bubble length (from the leading tip to the trailing edge of the bubble) and contact angle. As the measurement is easily affected by some noise or fluctuations of the operations, more than 600 bubbles were measured and analyzed to ensure the data reliable. The measurement error of dislodging pressure for the bubbles is below 10%.

Results and discussions

When bubble flows in a capillary network, it may lodge at some points of the microchannels due to the sudden change in channel size or angle, surface

roughness or fluids interactions, etc. Dislodgment of the trapped bubbles has been investigated in simple microchannels or networks, such as straight microchannels or microvessels[13, 15-16, 45, 48], the Y-type channels[14, 22, 49]. In this paper, experiments were designed to quantitatively investigate what factors affecting the dislodging pressure and bubble dislodgment behavior in a capillary network with asymmetric bifurcations, particularly the effect of bubble length, network structure and channel dimension on the dislodging pressure.

Effect of bubble length on dislodging pressure

The dislodging pressure for bubbles with different lengths in the same channel of the capillary network was plotted in Figs. 2 and 3. The graphs clearly demonstrate that there is a critical bubble length (about 2 mm in this study). When the bubble length is less than the critical length, the dislodging pressure for smaller bubbles is greater than that for bubbles with a larger length in the same channel, and the dislodging pressure increases with the decrease of bubble length. Once the bubble length is greater than 2 mm, the dislodging pressure is almost constant and independent of the bubble length.

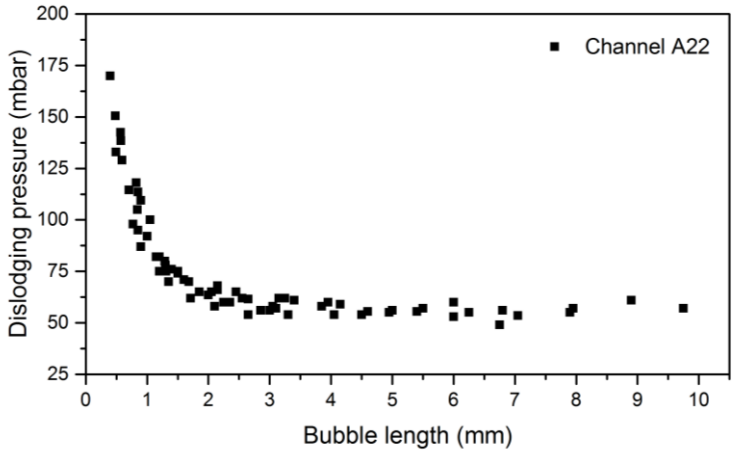

Fig. 2 Dislodging pressure for bubbles with different lengths in channel A22

Fig. 2 shows bubble dislodging pressure profile in the channel A22. The same trend has been observed in all other channels of the capillary network, but the magnitude of dislodging pressure varies significantly with channels. For example, in Figs 2 and 3, the dislodging pressure for a bubble with a length of 1 mm is about 92 mbar in channel A22, 32 mbar in channel A11, 47.5 mbar in channel A21, and 20 mbar in channel B11. The significant difference in the dislodging pressure is not only caused by the channel dimension, but also the network structure. This will be discussed in next section.

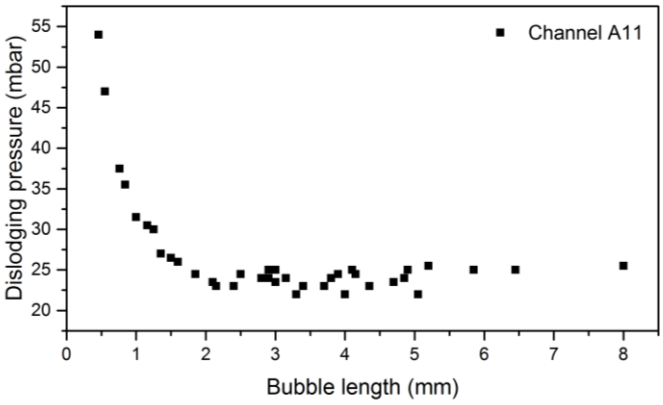

(a)

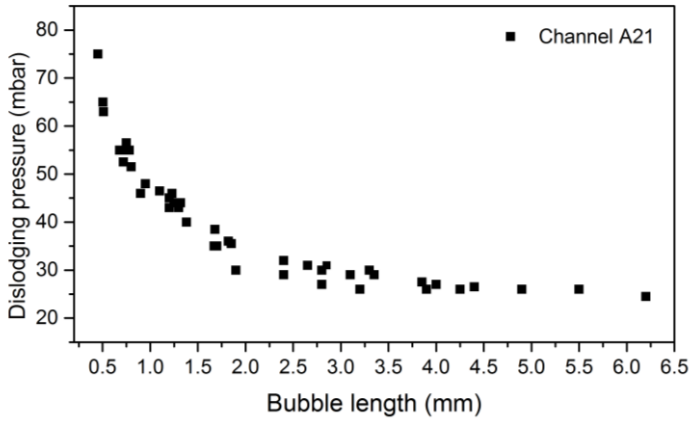

(b)

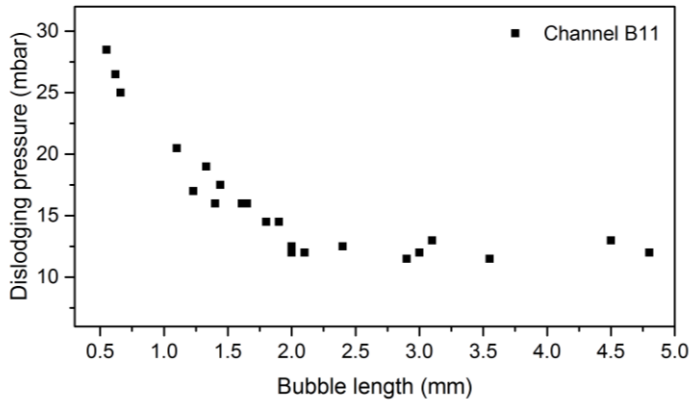

(c)

Fig. 3 Dislodging pressure for bubbles with different lengths in channel (a) A11 (b) A21 and (c) B11

To authors' best knowledge, this relationship between the dislodging pressure and bubble length in a complex capillary network has not been reported yet. Very few study has been conducted to measure dislodging pressure for bubbles with a length in a large range in a microscopic capillary network. Blackmore et al. and Daniel et al. reported that smaller bubbles require a higher dislodging pressure in a straight channel[15, 45]. Both two groups did not illustrate the explicit relationship between the dislodging pressure and bubble length. Daniel et al. demonstrated that a higher liquid flow rate is required to dislodge smaller

bubbles as smaller bubbles have less contact force due to the smaller surface area. They simply lumped all forces acting on the bubble as the contact force, which is too vague to represent the complicated forces involved in bubble dislodgement.

Effect of network structure and channel size on bubble dislodging pressure

The diverging/converging angles of bifurcations, channel dimension and the complexity of the flowpath affect the bubble dislodging pressure through affecting energy loss and fluid velocity. In this study, as $1<Re<10$, the inertia of the liquid cannot be neglected compared with viscous effect[50-52]. When the liquid flows through a channel with curvature, the liquid inertia will contribute to the velocity mismatch in the downstream direction between the liquid in the central and near-wall regions. The velocity mismatch causes the energy dissipation, and thus the liquid velocity will be smaller in the channel with curvature than the velocity in straight channel under the same injection flowrate. As the driving force is proportional to the liquid velocity, the driving force to dislodge the bubble is smaller in a curved channel. For a bubble with same volume, the dislodging pressure provided at the network inlet will be higher in order to dislodge a bubble in a curved channel than in a straight channel.

Network structure

The effect of network structure on the bubble dislodging pressure is discussed in terms of diverging/converging angle and complexity of flowpath. The diverging angle of bifurcations is defined as the angle between the diverging fluid and the parent fluid velocity vector as illustrated in Figs. 4b, 5b and 7b. Converging angle is defined in similar way and shown in Fig. 4d.

Figs. 4-7 compare the dislodging pressure among different channels, and demonstrate how the impact of bubble length on the dislodging pressure varies with network structure. From the dislodging pressure profiles for channels with similar size and flow condition, we found that the larger the diverging angle and/or converging angle, the higher the pressure is required to dislodge a bubble with the same length.

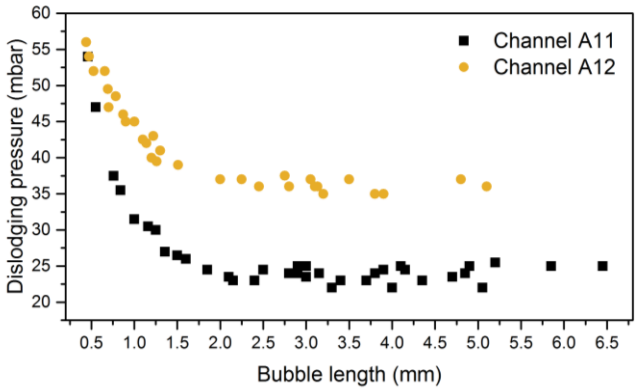

(a)

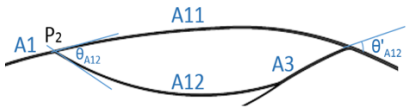

(b)

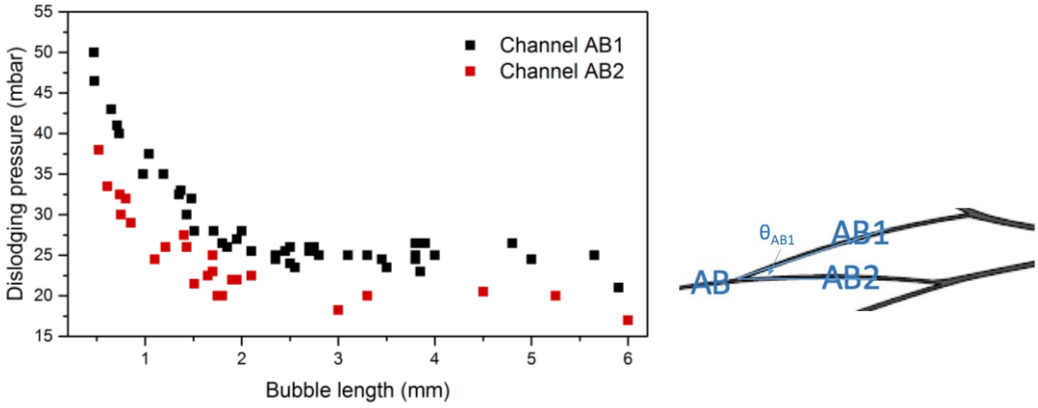

(c) (d)

Fig. 4 (a) Dislodging pressure profiles for bubbles in channels A11 (*W*=0.46 mm) and A12 (*W*=0.46 mm); (b) a schematic diagram of channels A11 and A12; (c) dislodging pressure profiles for bubbles in channels AB1 and AB2; and (d) a schematic diagram of channels AB1 and AB2. (θ_{A12} is the diverging angle of channel A12, θ'_{A12} is the converging angle of channel A12, and θ_{AB1} is the diverging angle of channel AB1)

For example, the dislodging pressure for bubbles in channel A12 is significantly higher than that in channel A11 as shown in Fig. 4a. Considering that channels A11 and A12 have similar size (*W*≈0.46 mm, *H*≈0.32 mm) and they share the same inlet (A1) and outlet (A4), the main difference between two channels is the diverging angle (θ_{A12}≈40.8º and θ_{A11}≈0º) and converging angle (θ'_{A12}≈48º and θ'_{A11}≈0º). Similarly, channels AB1 and AB2 have similar size (*W*≈0.45 mm, *H*≈0.32 mm), and they share the same inlet (channel AB), as shown in Fig. 4d. The dislodging pressure in channel AB1 is greater than that in channel AB2,

and the diverging angle of channel AB1 (θ_{AB1}≈14.4°, θ_{AB2}≈0°) is slightly larger. The comparison of channels A11 and A12, channels AB1 and AB2 indicates that the diverging and converging angle may have effect on the bubble dislodging pressure in network.

To demonstrate the angle effect, we employed the electric circuit analogy to predict the pressure drop across the single channel where the bubble lodges. The circuit method is based on the analogous behavior of hydraulic electric circuits, with correlations of pressure to voltage, volumetric flowrate to current, and hydraulic resistance to electric resistance. The hydraulic resistance (R_H) for the rectangular microchannel can be predicted theoretically according to equation (4)[53-54]. As the capillary effect dominates the flow of the blocked channel (Ca~10^{-4}), the resistance of the blocked channel is significantly higher than the resistance of other channels. The channel in which the bubble lodges/blocks can be analogized to a resistor with infinite electric resistance. The equivalent electric circuit and equivalent resistors are shown in Fig. S1. The pressure across the blocked channel then can be predicted through Simulink, Matlab. For example, the pressure difference between the two ends of channel A11 (ΔP_{A11}) can be calculated through equation (5),

$$R_H = \frac{12\sigma L}{wh^3\{1-\frac{h}{w}[\frac{192}{\pi^5}\sum_{n=1,3,5}^{\infty}\frac{1}{n^5}\tanh(\frac{n\pi w}{2h})]\}} \quad (4)$$

$$\Delta P_{A11} = \Delta P_{total} - Q_A R_{H(A)} - Q_{A1} R_{H(A1)} - Q_{A4} R_{H(A4)} - Q_{A5} R_{H(A5)} \quad (5)$$

where w, h and L are the microchannel width, height and length, respectively, ΔP_{total} is the experimental overall pressure required to dislodge one bubble

from channel A11.

Similarly, pressure difference between the two ends of channel A12, AB1 and AB2 when dislodging one bubble from the corresponding channel can be obtained following the same procedure. The data are shown in Table S1, which indicates that $\Delta P_{A12} > \Delta P_{A11}$ and $\Delta P_{AB1} > \Delta P_{AB2}$ when the bubble lengths in these channels are the same. The main difference between two sets of channels is the diverging angle (θ_{A12}≈40.8º> θ_{A11}≈0º and θ_{AB1}≈14.4º> θ_{AB2}≈0º) and converging angle (θ'_{A12}≈48º> θ'_{A11}≈0º). Therefore, the comparison of pressure across the single channels of A11 and A12, and channels of AB1 and AB2 demonstrated that the diverging angle and converging angle affects the dislodging pressure in complex network.

Another factor affecting the bubble dislodging pressure is the complexity of flowpath. It is easy to understand that the fluid is prone to choose the relatively easier way to travel under the same flow rate, as more energy would be lost to travel through a complex flowpath. For example, channel A22 (*W*=0.37 mm) and channel A21 (*W*=0.26 mm) have the same inlet (channel A2), and the diverging angle is similar (θ_{A21}≈θ_{A22}≈7.8º), while the dislodging pressure in channel A22 is larger than that in channel A21 as shown in Fig. 5a. This is mainly attributed to the network complexity, i.e. the existence of the channels AB, AB1 and AB2.

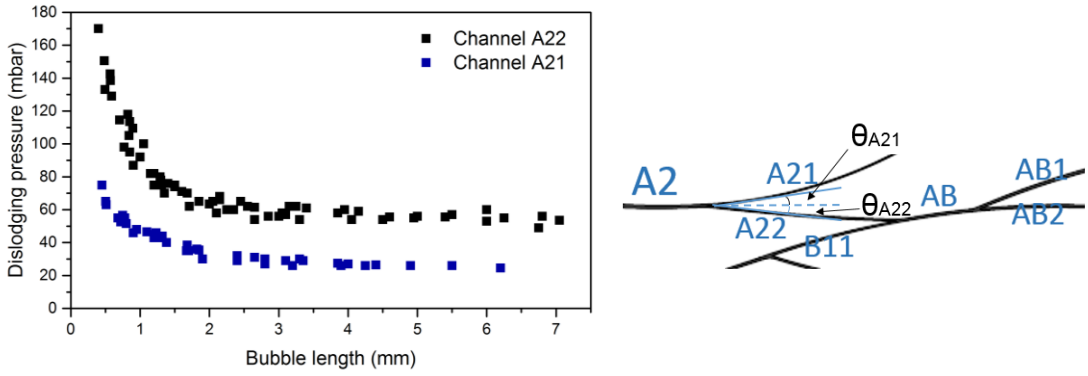

(a) (b)

Fig. 5 (a) Dislodging pressure profiles for bubbles in channels A21 and A22; (b) a schematic diagram of the network structure around channel A21 and A22 (θ_{A21} and θ_{A22} is the diverging angle of channel A21 and A22, respectively)

Channel size

In a single capillary, narrower channel will give a higher resistance to bubble movement based on the reciprocal relationship between the channel diameter and pressure drop. However, this may not occur in complex capillary network with high interconnectivity, and the comprehensive effect induced by the complex structure and multichannel features is required to be taken into account when analyzing the bubble dislodgement.

The effect of channel size in this capillary network is not obvious due to the effect of network structure. For example, channels A22 and B11 have a width of about 0.36 mm, but the bubble dislodging pressure in channel A22 is significantly higher than that in channel B11 as shown in Fig. 6. Similar

phenomenon has been discussed above in channels A11- A12 and channels AB1- AB2 (Fig. 4).

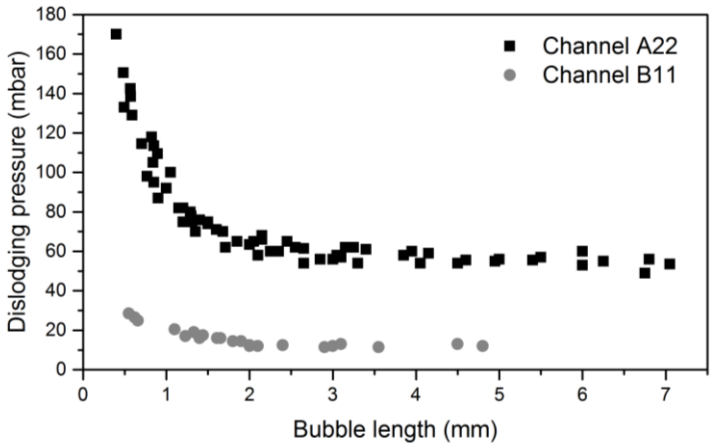

Fig. 6 Dislodging pressure profiles for bubbles in channels B11 (*W*=0.36 mm) and A22 (*W*=0.37 mm)

The interplay between the impact of network structure and the impact of channel size on the dislodging pressure varies with the bubble length. Taking channels A21 (*W*=0.26 mm) and A12 (*W*=0.46 mm) as an example, they have the same converged channel (A3), but different inlet channels. Theoretically, the narrower channel (channel A21) should provide a higher resistance to bubble movement. However, as shown in Fig. 7a, when bubble length is larger than around 1.5 mm, the dislodging pressure in channel A12 (wider) is higher than that in channel A21 (narrower). It seems that for large bubbles, the dislodging pressure is dominated by network structure, rather than the channel width. The fluid loses more energy from P1 (as shown in Fig. 7b) to reach channel A12 due to the high diverging angle in P2 ($\theta_{A12}\approx40.8^{o}$), and loses less

energy to reach channel A21 due to the lower diverging angle (θ_{A21}=7.8º) at P3. For bubbles with a length less than 1.5 mm, the dislodging pressure for bubbles with a similar length in channel A21 (narrower) is higher than that in channel A12 (wider), which is opposite to the dislodging pressure profile for bubbles with a length greater than 1.5 mm. The pressure increase rate in channel A21 is larger than that in channel A12. For example, when the bubble length decreases from 3.1 mm to 0.5 mm, the dislodging pressure increases from 37.5 mbar to 55 mbar in channel A12, and from 28.5 mbar to 75 mbar in channel A21. This indicates that the channel width influences significantly the dislodging pressure increase rate when the bubble length is less than 1.5 mm. Narrower channels will be more sensitive to the change of bubble length. Further explanation of these phenomena based on our proposed model has been detailed in next section.

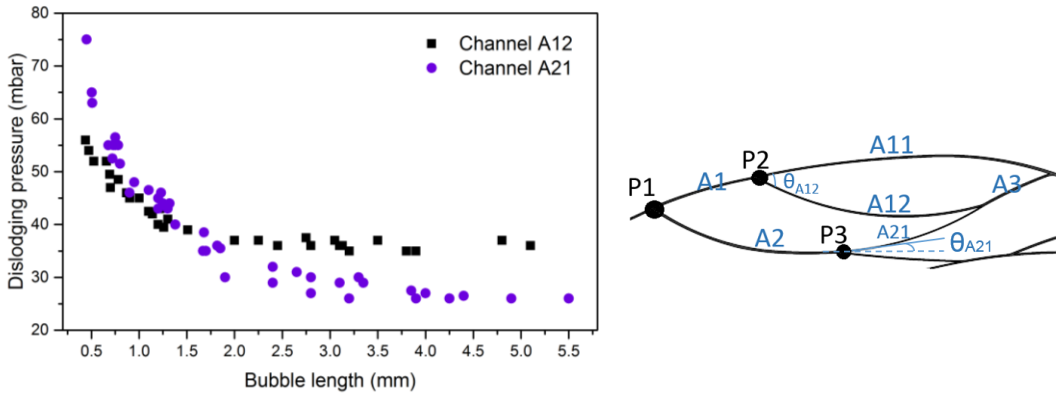

(a) (b)

Fig. 7 (a) Dislodging pressure for bubbles with different lengths in channels A12 (*W*=0.46 mm) and A21 (*W*=0.26 mm); (b) a schematic diagram of the network

structure around channels A12 and A21, and θ_{A21} is the diverging angle of channel A21

Modelling

The bubble dislodgement in a capillary network is complicated. It involves the effects of bubble length, channel size, network structure, interfacial tension between liquid and gas, the wettability of network material, etc. To consider the influence of network structure, i.e. multi-channel, multi-bifurcation and bifurcating angles, a parameter c_j is proposed to represent the contribution of the dislodging pressure from the individual channel *j* in the network.

Full model

A theoretical model is proposed to describe the behavior of bubble dislodgement from a microchannel in complex capillary network. Considering the moment when the motion of the bubble is initiated, a bubble slug as shown in Fig. 8 is selected for following discussion.

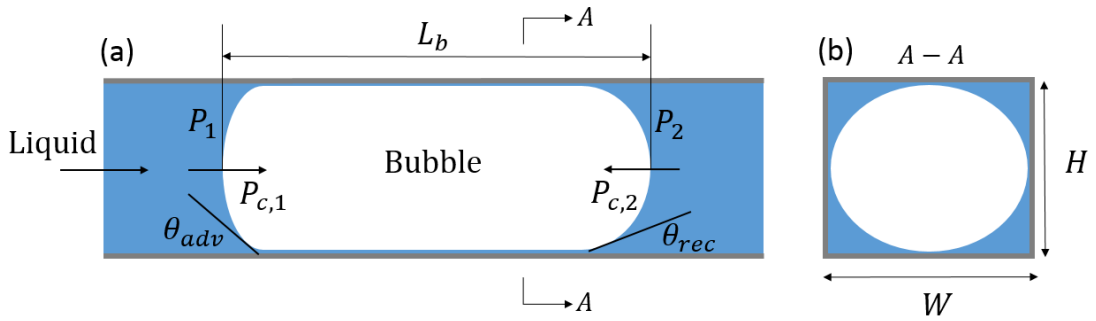

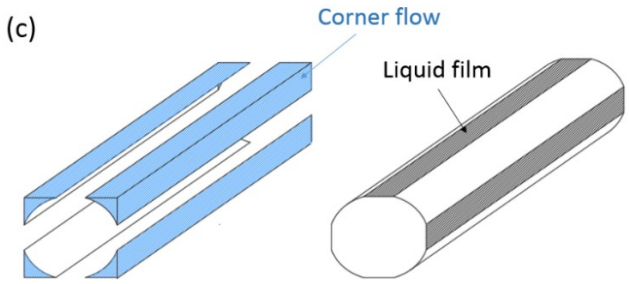

Fig. 8 (a) A schematic diagram of bubble slug in a microchannel of the capillary network in its static state, (b) a cross-sectional view of the gas/liquid distribution across the channel, and (c) a schematic diagram of the bubble flow through a microchannel in which liquid flows past the bubble through the corner

We assume that the pressure drop through the bubble slug is equal to the pressure difference between the pressure in bubble left end (P_1) and pressure in bubble right end (P_2), i.e.,

$$\Delta P_{bubble} = P_1 - P_2 \quad (6)$$

By applying a driving pressure to the bubble, the shape of the bubble will be deformed first to against the bubble movement, thus a capillary pressure drop is induced due to the difference between the left and right curvatures[16, 38]. The frictional force exists between the liquid film and the bubble phase, acting as another resistant force for bubble moving[40]. The resistant pressure drop for the bubble movement (ΔP_{bubble}) is thus the sum of the frictional pressure drop (ΔP_f) and the capillary pressure drop (ΔP_c), i.e.,

$$\Delta P_{bubble} = \Delta P_f + \Delta P_c \quad (7)$$

The capillary pressure drop is calculated by equation (1). The frictional pressure drop caused by the liquid film can be calculated based on the Darcy-Weisbach equation which shows a good prediction in several previous studies[35, 55-57]. In the bubble slug unit, the frictional pressure drop ΔP_f can be written based on equation (2)[8, 35, 41] as,

$$\Delta P_f = 2\rho_l f_f u_b^2 \frac{l_b}{H_j} \tag{8}$$

where ρ_l is the density of DI water, u_b is the mean superficial velocity of bubble, l_b is the length of bubble slug (bubble length) and H_j is the height of the corresponding microchannel.

The driving pressure around the bubble is maintained by the corner flow, as the corner liquid (the blue section, as depicted in Figs. 8b and 8c) drags the bubble to move. The pressure drop for the corner flow is equal to the driving pressure exerting on the bubble, which was also assumed by Wong et al. and Mohammadi[16, 38]. As the liquid flowing across the corner can be treated as Poiseuille flow, the pressure drop for the corner flow can be approximately calculated based on Poiseuille law, gives as,

$$P_1 - P_2 = \frac{128\mu_l l_b Q_f}{\pi D_{eff}^4} \tag{9}$$

where μ_l is the viscosity of DI water, Q_f is volumetric flow rate and D_{eff} is the effective dynamic diameter of the liquid flow in corners which can be assumed as a constant for each microchannel in this study.

In this capillary network, the volumetric flow rate Q_f is the function of the pressure difference between inlet and outlet of the microchannel (ΔP_j), and can be expressed according to the Darcy's law[58],

$$Q_f = -\frac{KK_{r,f}A}{\mu_l}\frac{\partial p}{\partial x} = \frac{KK_{r,f}A_j}{\mu_l}\frac{\Delta P_j}{L_j} \quad (10)$$

$$\Delta P_j = c_j * \Delta P$$

Where *K* is the absolute permeability of the microchannel, $K_{r,f}$ is the relative permeability of fluid, *A* is the sectional area of the microchannel, *L* is the length of the microchannel, ΔP_j is the pressure drop in microchannel *j*, ΔP is the overall pressure difference between the inlet and outlet of the capillary network. Parameter c_j, a pressure loss factor of the corresponding microchannel *j*, is defined to characterize the pressure loss caused by network structures (such as multi-channel, multi-bifurcation, bifurcating angles), gives as, $c_j = \frac{\Delta P_j}{\Delta P}$. It can be seen as the contribution of the dislodging pressure in the individual channel *j* in the network.

Combining equations (6) - (10), the pressure difference initiating the bubble movement can be expressed as,

$$\Delta P = \frac{\pi D_{eff}^4 L_j}{64KK_{r,f}W_jH_jc_j}\left[\frac{\sigma(\frac{1}{W_j}+\frac{1}{H_j})(\cos\theta_{rec}-\cos\theta_{adv})}{l_b} + \frac{\rho_l f_f u_b^2}{H_j}\right] \quad (11)$$

The relative permeability $K_{r,f}$ is related to the void fraction (the fraction of the channel cross-sectional area that is occupied by the bubble, as shown in Fig. 8b), and it can be approximately taken as an invariable. The difference in the cosine of the receding and advancing angle changes in a small range, which can be roughly neglected.

The equation (11) can be written as a simple form,

$$\Delta P = \frac{MA_j}{l_b} + NB_j \quad (12)$$

in which, $A_j = \frac{L_j}{W_j H_j c_j}\left(\frac{1}{W_j} + \frac{1}{H_j}\right)$, $B_j = \frac{L_j}{W_j H_j^2 c_j}$ (13)

$$M = \frac{\sigma \pi D_{eff}^4}{64KK_{r,f}}(\cos\theta_{rec} - \cos\theta_{adv}),\ N = \frac{\pi D_{eff}^4 \rho_l f_f u_b^2}{64KK_{r,f}} \quad (14)$$

where A_j and B_j are the parameters related to the corresponding microchannel, and *M* and *N* are constant for the same microchannel.

Analysis of experimental results

The model proposed in equation (11) fully describes the factors affecting dislodging pressure for single bubble in a capillary network with multi-channel and multi-bifurcation. It closely relates to the channel dimension (width, length and height), bubble length, fluid flow rate, contact angle, and network structure. The impact of network structure and channel size on the dislodging pressure has been discussed quantitatively. In this section, experimental results will be analysed through combining the model with parameters MA_j, NB_j as well as parameter c_j.

This model demonstrates that the dislodging pressure is dependent on the bubble length (l_b) in a complex capillary network. For bubbles with small lengths, the dislodging pressure increases significantly with the decrease of bubble length, i.e. smaller bubble will require higher pressure to dislodge. When the bubble length is longer than a certain value, the dislodging pressure is nearly equal to a constant (NB_j) and is independent of bubble length for a fixed

channel and flow conditions. This model matches very well with our experimental results, and dislodging pressure profile for every channel in this network fits equation (12) with a very high R-Square value, as shown in supporting materials (Fig. S2).

Equation (12) illustrates that parameter MA_j corresponds to the increase rate of the dislodging pressure, and parameter NB_j is the dislodging pressure of bubbles with infinite length (the nearly horizontal section of the pressure profile). The ratio of parameter MA_j and NB_j for each channel can be obtained from experimental dislodging pressure. Fig. 9 indicates that the ratio of parameters (MA_j/NB_j) varies linearly with $H_j(\frac{1}{W_j}+\frac{1}{H_j})$, which is in good agreement with the correlation (13) derived based on the equation (12).

$$\frac{MA_j}{NB_j} = CH_j(\frac{1}{W_j}+\frac{1}{H_j}), \tag{15}$$

in which *C* is a constant for the corresponding channel *j*.

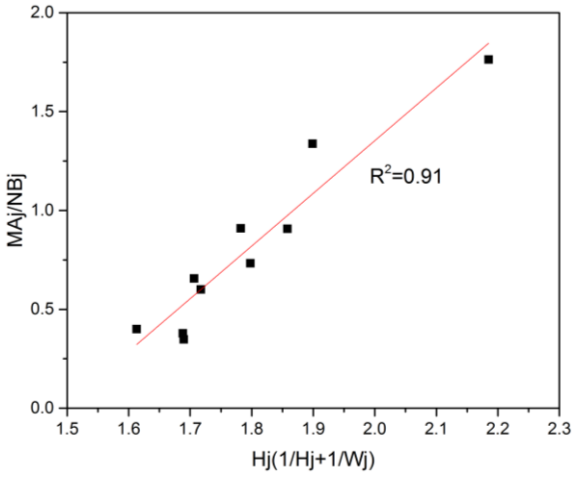

Fig. 9 A plot of the parameter ratio of MA_j/NB_j versus the dimensionless constant $H_j(\frac{1}{W_j}+\frac{1}{H_j})$, the red line represents the best fit line

According to equation (11), parameters MA_j and NB_j are both proportional to channel length (*L*), and reversely proportional to channel size (*W* and *H*) and parameter c_j. Parameter c_j characterizes the effect of the network structure, i.e. multichannels, multi-bifurcations and channel complexity, on the dislodging pressure. A small magnitude of parameter c_j indicates the impact of network structure on the dislodging pressure is significant. In Fig. 10a, channels A12, A22, and B12 have relatively high parameter NB_j among other channels. These three channels are not characterized by the longest length or smallest channel size. The relatively high value of parameter NB_j is attributed to the smaller value of parameter c_j due to the bifurcating angles. The magnitude of NB_j for channel A11 and channel A21 is not noticeably high even though channel A11 has the longest length and channel A21 has the smallest channel size. These indicate that the impact of channel size and channel length on the parameter NB_j is not obvious. Therefore, parameter c_j, rather than channel dimension dominates the magnitude of NB_j of microchannels in a capillary network. In other words, the network structure, rather than channel dimension dominates the dislodging pressure for bubbles with long length in a complex capillary network.

Although channel size does not markedly affect the magnitude of NB_j, it takes more effect on the parameter MA_j. As shown in equation (13), parameter MA_j is inversely proportional to W^2 (channel width), while parameter NB_j is only

affected by *W*. From Fig. 10b, channel A21 has the second largest magnitude of MA_j (around 33 mbar·mm), even though the c_j value of channel A21 is large and the length of channel A21 is small (L_{A21}=2.95 cm). The reason for the large MA_j of channel A21 is the smallest channel width (W_{A21}=0.26 mm), i.e. the channel width affects MA_j significantly.

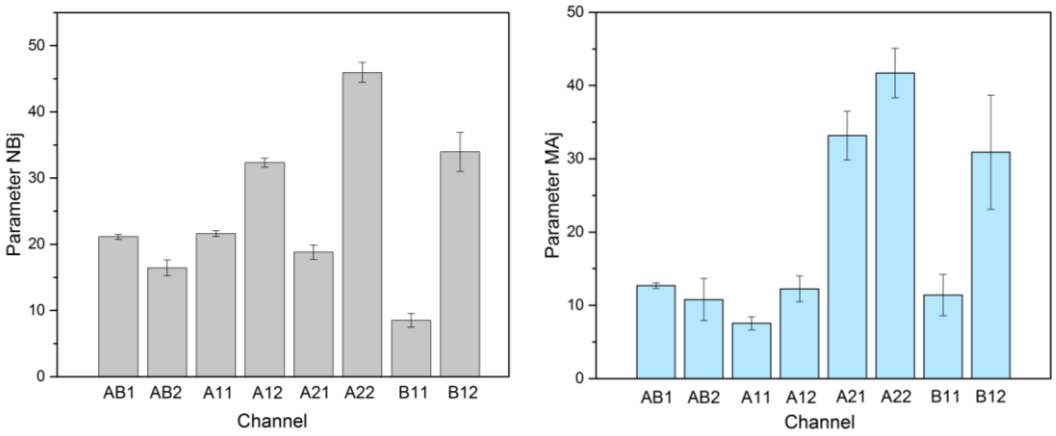

(a) (b)

Fig. 10 Comparison of (a) parameter NB_j and (b) MA_j among different channels in the capillary network

The analysis of parameter MA_j, NB_j and c_j has clearly explained the experimental data, and the effect of bubble length and network structure on the dislodging pressure in previous sections. For example, for bubbles with a large length, dislodging pressure for bubbles in channel A12 is higher than that in channel A21 (as shown in Fig. 7a) due to the dominant impact of network structure. This explanation agrees well with the analysis of parameter NB_j (corresponding to the dislodging pressure for long bubbles), which is

dominated by the parameter c_j. For bubbles with small length, the dislodging pressure in channel A21 becomes higher than that in channel A12 owing to the effect of channel width. This is in line with the analysis of parameter MA_j as the dislodging pressure of small bubble is significantly affected by the increase rate (i.e. parameter MA_j), which highly depends on channel width.

Conclusions

The bubble dislodgement in complex capillary network has been investigated in terms of the bubble length, diverging/converging angle, channel complexity and channel dimensions (length, height and width). The dislodging pressure profiles demonstrate that there is a critical bubble length for every microchannel of the network. When the bubble length is less than this critical value, dislodging pressure will increase with the decrease of the bubble length, i.e. smaller bubbles require higher dislodging pressure. Once the bubble length is longer than the critical value, the dislodging pressure is independent of bubble length. Every channel of the capillary network has similar trend of dislodging pressure-bubble length profile. Furthermore, the effect of the diverging/converging angle and channel size have been investigated through comparing the dislodging pressure profiles among different channels. Generally, higher dislodging pressure is required for bubbles with same length in the channel with diverging/converging angles.

A one-dimensional model has been derived to fully describe the bubble

dislodgement in complex capillary network, and to predict the dislodging pressure. Parameter c_j is introduced to characterize the effect of network structure (i.e. multichannel and multi-bifurcation features) on the dislodging pressure. The model agrees well with the experimental results. In this capillary network, parameter NB_j is dominated by parameter c_j (network structure effect) and the increase rate of the dislodging pressure (parameter MA_j) is affected significantly by both the channel width and parameter c_j. This model has been validated and could be employed in other capillary networks.

Supporting information

Schematic of the equivalent fluidic circuit and fluidic resistors; Table of pressure difference across single channels; Diagrams of dislodging pressure profiles for bubbles in each channel of the complex capillary network.

Reference

1. Farajzadeh, R.; Andrianov, A.; Krastev, R.; Hirasaki, G. J.; Rossen, W. R., Foam-oil interaction in porous media: Implications for foam assisted enhanced oil recovery. *Adv. Colloid Interface Sci.* 2012, *183*, 1-13.
2. Bull, J. L., Cardiovascular bubble dynamics. *Crit. Rev. Biomed. Eng.* 2005, *33* (4), 299-346.
3. Valassis, D. T.; Dodde, R. E.; Esphuniyani, B.; Fowlkes, J. B.; Bull, J. L., Microbubble transport through a bifurcating vessel network with pulsatile flow. *Biomed. microdevices* 2012, *14* (1), 131-43.
4. Yang, H.; Zhao, T. S.; Ye, Q., In situ visualization study of CO2 gas bubble behavior in DMFC anode flow fields. *J. Power Sources* 2005, *139* (1-2), 79-90.
5. Calabriso, A.; Borello, D.; Romano, G. P.; Cedola, L.; Del Zotto,

L.; Santori, S. G., Bubbly flow mapping in the anode channel of a direct methanol fuel cell via PIV investigation. *Appl. Energy* **2017,** *185*, 1245-1255.
6. Steinbrenner, J. E.; Lee, E. S.; Hidrovo, C. H.; Eaton, J. K.; Goodson, K. E., Impact of channel geometry on two-phase flow in fuel cell microchannels. *J. Power Sources* **2011,** *196* (11), 5012-5020.
7. Chen, X. Y.; Zhang, Z.; Yi, D. L.; Hu, Z. L., Numerical studies on different two-dimensional micromixers basing on a fractal-like tree network. *Microsyst. Technol.* **2017,** *23* (3), 755-763.
8. Yue, J.; Chen, G. W.; Yuan, Q., Pressure drops of single and two-phase flows through T-type microchannel mixers. *Chem. Eng. J.* **2004,** *102* (1), 11-24.
9. Boehm, T.; Folkman, J.; Browder, T.; O'reilly, M. S., Antiangiogenic therapy of experimental cancer does not induce acquired drug resistance. *Nature* **1997,** *390* (6658), 404.
10. Bull, J. L., The application of microbubbles for targeted drug delivery. *Expert Opin. Drug Deliv.* **2007,** *4* (5), 475-93.
11. Samuel, S.; Duprey, A.; Fabiilli, M. L.; Bull, J. L.; Fowlkes, J. B., In vivo microscopy of targeted vessel occlusion employing acoustic droplet vaporization. *Microcirculation* **2012,** *19* (6), 501-9.
12. Hernot, S.; Klibanov, A. L., Microbubbles in ultrasound-triggered drug and gene delivery. *Adv. Drug Deliv. Rev.* **2008,** *60* (10), 1153-66.
13. Suzuki, A.; Eckmann, D. M., Embolism bubble adhesion force in excised perfused microvessels. *Anesthesiology* **2003,** *99* (2), 400-8.
14. Calderón, A. J.; Heo, Y. S.; Huh, D.; Futai, N.; Takayama, S.; Fowlkes, J. B.; Bull, J. L., Microfluidic model of bubble lodging in microvessel bifurcations. *Appl. Phys. Lett.* **2006,** *89* (24), 244103.
15. Blackmore, B.; Li, D. Q.; Gao, J., Detachment of bubbles in slit microchannels by shearing flow. *J. Colloid Interface Sci.* **2001,** *241* (2), 514-520.
16. Mohammadi, M.; Sharp, K. V., The Role of Contact Line (Pinning) Forces on Bubble Blockage in Microchannels. *J. Fluids Eng.* **2015,** *137* (3), 0312081-312087.
17. Banerjee, S.; Hassenklover, E.; Kleijn, J. M.; Cohen Stuart, M. A.; Leermakers, F. A., Interfacial tension and wettability in water-carbon dioxide systems: experiments and self-consistent field modeling. *J. Phys. Chem. B* **2013,** *117* (28), 8524-35.
18. Schäffer, E.; Wong, P.-z., Contact line dynamics near the pinning threshold: A capillary rise and fall experiment. *Phys. Rev. E* **2000,** *61* (5), 5257.
19. Calderon, A. J.; Eshpuniyani, B.; Fowlkes, J. B.; Bull, J. L., A boundary element model of the transport of a semi-infinite bubble through a microvessel bifurcation. *Phys. Fluids* **2010,** *22* (6), 61902.
20. Calderón, A. J.; Fowlkes, J. B.; Bull, J. L., Bubble splitting in

bifurcating tubes: a model study of cardiovascular gas emboli transport. *J. Appl. Physiol.* **2005,** *99* (2), 479-487.
21. Carlson, A.; Do-Quang, M.; Amberg, G., Droplet dynamics in a bifurcating channel. *Int. J. Multiph. Flow* **2010,** *36* (5), 397-405.
22. Eshpuniyani, B.; Fowlkes, J. B.; Bull, J. L., A bench top experimental model of bubble transport in multiple arteriole bifurcations. *Int. J. Heat Fluid FL.* **2005,** *26* (6), 865-872.
23. Escher, W.; Michel, B.; Poulikakos, D., Efficiency of optimized bifurcating tree-like and parallel microchannel networks in the cooling of electronics. *Int. J. Heat Mass Transf.* **2009,** *52* (5-6), 1421-1430.
24. Senn, S. M.; Poulikakos, D., Tree network channels as fluid distributors constructing double-staircase polymer electrolyte fuel cells. *J. Appl. Phys.* **2004,** *96* (1), 842-852.
25. Chen, Y. P.; Zhang, C. B.; Wu, R.; Shi, M. H., Methanol steam reforming in microreactor with constructal tree-shaped network. *J. Power Sources* **2011,** *196* (15), 6366-6373.
26. Gosselin, L., Optimization of tree-shaped fluid networks with size limitations. *Int. J. Therm. Sci.* **2007,** *46* (5), 434-443.
27. Bello-Ochende, T.; Liebenberg, L.; Meyer, J. P., Constructal cooling channels for micro-channel heat sinks. *Int. J. Heat Mass Transf.* **2007,** *50* (21-22), 4141-4150.
28. Da Silva, A. K.; Bejan, A., Constructal multi-scale structure for maximal heat transfer density in natural convection. *Int. J. Heat Fluid FL.* **2005,** *26* (1), 34-44.
29. Chen, Y. P.; Deng, Z. L., Gas flow in micro tree-shaped hierarchical network. *Int. J. Heat Mass Transf.* **2015,** *80*, 163-169.
30. Wong, H.; Radke, C.; Morris, S., The motion of long bubbles in polygonal capillaries. Part 2. Drag, fluid pressure and fluid flow. *J. Fluid Mech.* **1995,** *292*, 95-110.
31. Kreutzer, M. T.; Kapteijn, F.; Moulijn, J. A.; Kleijn, C. R.; Heiszwolf, J. J., Inertial and interfacial effects on pressure drop of Taylor flow in capillaries. *AICHE J.* **2005,** *51* (9), 2428-2440.
32. Bento, D.; Sousa, L.; Yaginuma, T.; Garcia, V.; Lima, R.; Miranda, J. M., Microbubble moving in blood flow in microchannels: effect on the cell-free layer and cell local concentration. *Biomed Microdevices* **2017,** *19* (1), 6.
33. Eckmann, D. M.; Cavanagh, D. P., Bubble detachment by diffusion-controlled surfactant adsorption. *Colloid Surf. A* **2003,** *227* (1-3), 21-33.
34. Dussan, E. B.; Chow, R. T. P., On the Ability of Drops or Bubbles to Stick to Non-Horizontal Surfaces of Solids. *J. Fluid Mech.* **1983,** *137* (Dec), 1-29.
35. Younes, A.; Hassan, I.; Kadem, L., Investigation of Bubble Frequency for Slug Flow Regime in a Uniformly Heated Horizontal

Microchannel. *J Heat Trans-T Asme* **2017,** *139* (6), 061501.
36. Paust, N.; Litterst, C.; Metz, T.; Eck, M.; Ziegler, C.; Zengerle, R.; Koltay, P., Capillary-driven pumping for passive degassing and fuel supply in direct methanol fuel cells. *Microfluid. Nanofluid.* **2009,** *7* (4), 531-543.
37. Gaakeer, W. A.; de Croon, M. H. J. M.; van der Schaaf, J.; Schouten, J. C., Liquid-liquid slug flow separation in a slit shaped micro device. *Chem. Eng. J.* **2012,** *207*, 440-444.
38. Wong, C. W.; Zhao, T. S.; Ye, Q.; Liu, J. G., Transient capillary blocking in the flow field of a micro-DMFC and its effect on cell performance. *J. Electrochem. Soc.* **2005,** *152* (8), A1600-A1605.
39. Bretherton, F. P., The Motion of Long Bubbles in Tubes. *J. Fluid Mech.* **1961,** *10* (2), 166-188.
40. Ma, S. X.; Mason, G.; Morrow, N. R., Effect of contact angle on drainage and imbibition in regular polygonal tubes. *Colloid Surf. A* **1996,** *117* (3), 273-291.
41. Kawahara, A.; Chung, P. M. Y.; Kawaji, M., Investigation of two-phase flow pattern, void fraction and pressure drop in a microchannel. *Int. J. Multiph. Flow* **2002,** *28* (9), 1411-1435.
42. McAdams, W. H., *Heat transmission*. third ed.; McGraw-Hill: New York, 1954.
43. A. Cicchitti, C. L., M. Silvestri, G. Solddaini, R. Zavalluilli, Two-phase cooling experiments－Pressure drop, heat transfer and burnout measurement. *Energia Nucl.* **1960,** *7* (6), 407-425.
44. Dukler, A. E.; Wicks, M.; Cleveland, R. G., Frictional pressure drop in two－phase flow: A. A comparison of existing correlations for pressure loss and holdup. *AICHE J.* **1964,** *10* (1), 38-43.
45. Cavanagh, D. P.; Eckmann, D. M., Interfacial dynamics of stationary gas bubbles in flows in inclined tubes. *J. Fluid Mech.* **1999,** *398*, 225-244.
46. Gao, Y. R.; Drew, P. J., Determination of vessel cross-sectional area by thresholding in Radon space. *J. Cereb. Blood Flow Metab.* **2014,** *34* (7), 1180-7.
47. Chung, P. M.-Y.; Kawaji, M.; Kawahara, A.; Shibata, Y. In *Two-Phase Flow Through Square and Circular Microchannels: Effect of Channel Geometry*, ASME/JSME 2003 4th Joint Fluids Summer Engineering Conference, American Society of Mechanical Engineers: 2003; pp 1459-1467.
48. Fuerstman, M. J.; Lai, A.; Thurlow, M. E.; Shevkoplyas, S. S.; Stone, H. A.; Whitesides, G. M., The pressure drop along rectangular microchannels containing bubbles. *Lab Chip* **2007,** *7* (11), 1479-89.
49. Poornima, J.; Vengadesan, S., Numerical simulation of bubble transport in a bifurcating microchannel: a preliminary study. *J. Biomech. Eng.* **2012,** *134* (8), 081005.
50. Debus, J. D.; Mendoza, M.; Succi, S.; Herrmann, H. J., Energy

dissipation in flows through curved spaces. *Sci. Rep.* **2017,** *7*, 42350.
51. Zhang, J.; Yan, S.; Yuan, D.; Alici, G.; Nguyen, N. T.; Ebrahimi Warkiani, M.; Li, W., Fundamentals and applications of inertial microfluidics: a review. *Lab Chip* **2016,** *16* (1), 10-34.
52. Di Carlo, D., Inertial microfluidics. *Lab Chip* **2009,** *9* (21), 3038-46.
53. Oh, K. W.; Lee, K.; Ahn, B.; Furlani, E. P., Design of pressure-driven microfluidic networks using electric circuit analogy. *Lab Chip* **2012,** *12* (3), 515-545.
54. Kim, D.; Chesler, N. C.; Beebe, D. J., A method for dynamic system characterization using hydraulic series resistance. *Lab Chip* **2006,** *6* (5), 639-644.
55. Walsh, E.; Muzychka, Y.; Walsh, P.; Egan, V.; Punch, J., Pressure drop in two phase slug/bubble flows in mini scale capillaries. *Int. J. Multiph. Flow* **2009,** *35* (10), 879-884.
56. Chung, P. M. Y.; Kawaji, M., The effect of channel diameter on adiabatic two-phase flow characteristics in microchannels. *Int. J. Multiph. Flow* **2004,** *30* (7-8), 735-761.
57. Kreutzer, M. T.; Kapteijn, F.; Moulijn, J. A.; Heiszwolf, J. J., Multiphase monolith reactors: Chemical reaction engineering of segmented flow in microchannels. *Chem. Eng. Sci.* **2005,** *60* (22), 5895-5916.
58. You, L. X.; Liu, H. T., A two-phase flow and transport model for the cathode of PEM fuel cells. *Int. J. Heat Mass Transf.* **2002,** *45* (11), 2277-2287.